Preprint typeset in JINST style - HYPER VERSION

Liquid Argon TPC Signal Formation, Signal Processing and Reconstruction

B. Baller[a]

[a] *Fermi National Accelerator Laboratory,*
Batavia, IL, USA
E-mail: baller@fnal.gov

ABSTRACT: This document describes a software chain that is directed towards the goal of fully automated reconstruction of neutrino interactions in a Liquid Argon Time Projection Chamber (LArTPC). The chain includes wire signal processing, reconstruction of hits that represent charge deposited on wires, reconstruction of 2D line-like clusters of hits, reconstruction of 2D and 3D vertices and the method for assembling these objects to make 3D tracks. Identification of higher level reconstructed objects makes use of the charge associated with lower level objects. Lower level objects may then be modified using information obtained at later stages of reconstruction. Techniques for reconstructing MeV-scale particles in a LArTPC are presented.

KEYWORDS: liquid argon; TPC.

Contents

1. Introduction

THIS IS A JUMBLED LIST OF TOPICS THAT SHOULD BE MENTIONED IN A REAL INTRODUCTION.

The liquid argon time projection chamber (LAr TPC) is an ideal technology for observing low energy particles in a large volume.

Used in ICARUS[2], ArgoNeuT[3], LongBo, CAPTAIN, MicroBooNE[4], SBND, DUNE (TODO: Need citations). Reconstruct low energy neutrino interactions $\approx$ few GeV.

Efficient reconstruction of tracks with length greater than a centimeter (proton kinetic energy $\gtrsim$ 20 MeV) is feasible using standard techniques that are described in this report. This capability enables exploring the role of final state interactions and short range correlations in neutrino interactions. This limit can in principle be lowered by techniques described in section 8.

The techniques described in this report were developed over the last 8 years and are currently implemented in LArSoft.[5] All data shown in this document are real unless labeled “simulation”.

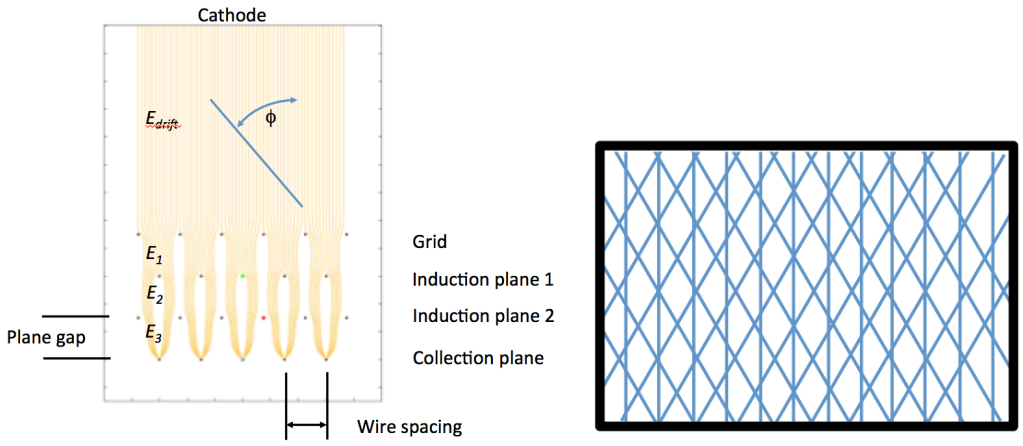

Figure 1. Left: Schematic view of the elements of a LArTPC in two dimensions. The blue line represents a track traveling at an angle ϕ relative to the electric field direction. Ionization electrons produced on the track follow the electric field lines (yellow) through the induction planes until they are collected on wires in the collection plane. Right: View of the wire planes as seen by the approaching electrons illustrating that the geometry of the left figure is overly simplistic.

2. Signal Formation

Electrons liberated by the passage of a minimum ionizing particle in a TPC are separated from their parent argon ions by $\approx 2\mu m$ after reaching thermal energies[6]. The electron and ion columns separate under the influence of an electric field, E_{drift}, that is typically < 1 kV/cm in a LArTPC. Electron-ion recombination occurs for the next few nanoseconds until the columns are well separated. The fraction of electrons that escape recombination is a strong function of the charge density and the electric field strength. The escape fraction, $\mathscr{R}$, can be modeled by a Birks "law" [8][9] or alternatively by the "Modified Box Model" [10] [11]. Both of these empirical models are based on the columnar theory of recombination by Jaffe [7]. The dependence on dE/dx is shown in Figure 3. The $\mathscr{R}$ values differ by less than 10% for $dE/dx < 35$ MeV/cm and approach 25% at 100 MeV/cm.

Electrons drift to the anode with a velocity of ≈ 1 mm/μs (see Figure 3) following the electric field lines as shown schematically in Figure 1. A fraction are lost during transport due to attachment on electro-negative impurities such as water and oxygen. The charge loss is characterized as a drift electron lifetime, τ_e. The ionization charge remaining after recombination, Q_o, is obtained from the collected charge at the wire planes, Q_c, using $Q_o = Q_c/\exp(-(t_{arrive} - t_o)/\tau_e)$ where t_{arrive} is the time of arrival of the electrons at the anode and t_o is the time of ionization event. Diffusion will increase the spatial extent of the electron cloud governed by $\sigma_D = 2\sqrt{D_{T(L)}(t_{arrive} - t_o)}$ where $D_{T(L)}$ is the longitudinal (transverse) diffusion coefficient.

The anode typically consists of several wire planes with bias voltages set so that ionization electrons travel between the wires of the induction planes inducing a bipolar signal. The charge is collected on the last plane, the collection plane. The wire plane bias voltage settings for transporting 100% of the ionization electrons to the collection plane is a function of the wire diameter, wire spacing and plane spacing[13][14]. The electric field between the wire planes should increase by approximately 50% for each successive plane gap to achieve full transparency. There is a concomi-

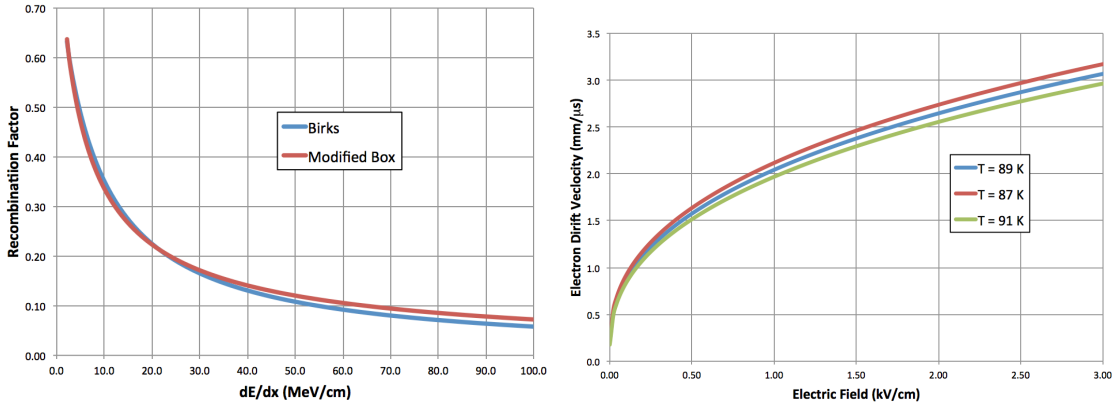

Figure 2. Left: Birks and modified Box Model parameterizations of electron recombination. Right: Parameterization of the drift velocity of electrons in LAr as a function of electric field and temperature from reference [12].

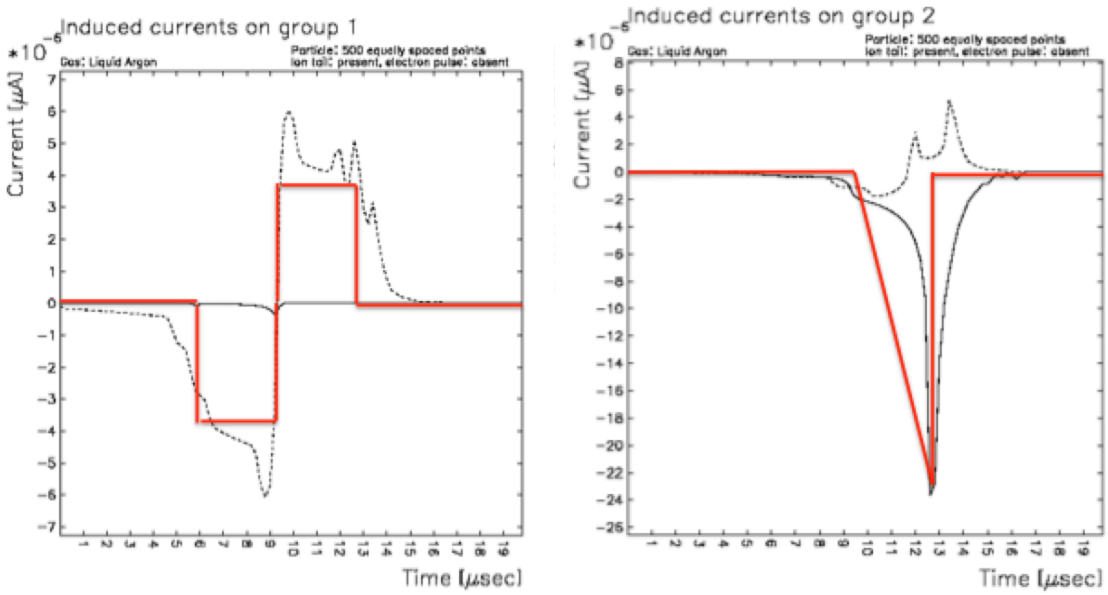

Figure 3. Left: Birks and modified Box Model parameterizations of electron recombination. Right: Parameterization of the drift velocity of electrons in LAr as a function of electric field and temperature from reference [12].

tant increase in the electron velocity of ≈15% which depends on the chosen value of E_{drift}. The wires in each plane are oriented relative to each other to provide a different view of the ionization event in each plane. The electrons therefore have a longer 3D trajectory through the wire planes than indicated by the 2D representation shown in Figure 1.

Signals formed on anode wires are dominated by the motion of ionization electrons occurring on the time scale of microseconds. The positive leading lobe of the signal induced on the first instrumented induction plane, the "U" plane, is negligible since the current induced on the wire occurs during the few milliseconds drift time of electrons in the meter-scale main volume. The

Table 1. Wire Configuration.

Detector	Wire planes and orientation TODO: CHECK
ArgoNeuT	Grid(0°), Induction(30°), Collection(-30°)
MicroBooNE	Induction(60°), Induction(-60°), Collection(0°)
(Proto) DUNE	Grid(0°), Induction(44°), Induction(-44°), Collection(0°)

negative trailing lobe is sizable since it is created from electrons traveling in the few mm gap between the U plane and the next plane, "V". These effects are illustrated in the MicroBooNE detector as shown in Figure 4. We will assume that there are three planes, U (induction), V (induction) and W (collection). In the following, the "Field response" refers to the time-dependent charge induced and collected due to the passage of ionization electrons through the wire planes.

The velocity of positive ions is significantly slower than that of electrons, approximately 5 mm/s, resulting in a positive ion buildup in the TPC, or "space charge", that can affect the function of long drift TPCs operated in a high rate of background ionization. The electrical circuit is complete when ions reach the cathode plane. This may be a few minutes in a 2 meter drift TPC.

The wire plane configurations for several Fermilab detectors are shown in Table 1, where Grid denotes an un-instrumented induction plane. A wire with 0° orientation is vertical. Using a grid plane restores the positive leading lobe effectively doubling the size of signals on the first instrumented induction plane. An additional benefit is that it protects against damage to readout electronics from electrostatic discharge during handling.

The number of wire planes and the wire orientation was chosen to optimize the competition between pattern recognition capability, electronics noise and cost. A LArTPC with three views is clearly more capable in resolving overlapping tracks than a detector with two views. TODO: THIS ISN'T THE PLACE TO TALK ABOUT NOISE, COST, ETC. MOVE IT ELSEWHERE OR DELETE.

ICARUS used charge integrating amplifiers on the middle induction plane to produce unipolar signals on the induction plane. Hits were reconstructed by fitting an analytical function to the raw wire signals. In contrast, the ArgoNeuT and MicroBooNE experiments elected to instrument all planes with the same electronics. Some level of offline signal processing is desirable for reconstructing hits in the V plane. We will use the term "electronics response" to refer to the output of the full readout electronics chain by the injection of a δ-function input.

Raw signals in the ArgoNeuT detector in Figure 5 show the effects of an impedance mismatch between the TPC wires and the readout electronics. The readout electronics were spare DZero (TODO: check with Carl) equipment that were lent to ArgoNeuT with the condition that they would not be altered. The right hand image in this figure shows the same event after deconvolution using the method described in the next section.

The charge collected on each wire is amplified, digitized at a few MHz and stored for offline signal processing and reconstruction. TODO: DELETE THIS?

Many of the approximate values mentioned in this section are calculated explicitly in an Excel spreadsheet that includes parameterizations of liquid argon properties such as those shown in Figure 3. This "LArTPC Calculator" is described in Appendix A.

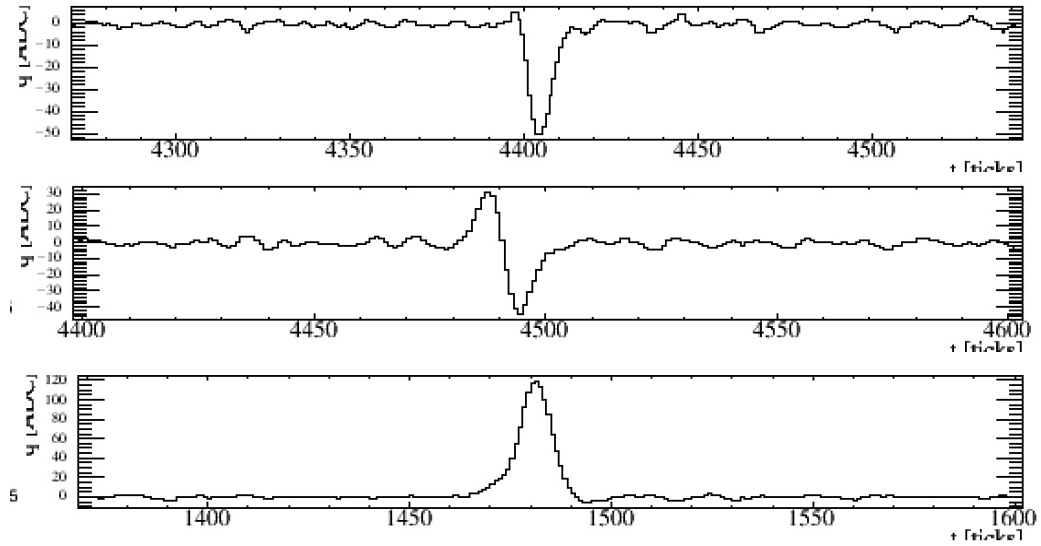

Figure 4. Pedestal-subtracted raw signals on a wire in the first induction plane (U, top), a wire in the second induction plane (V, middle) and a wire in the collection plane (W, bottom) in the MicroBooNE detector. The horizontal axes are the sample number in the TPC readout window, or "tick", where 1 tick = 0.5 μs in MicroBooNE. The vertical axes are the pedestal subtracted digitized signals (ADC counts) produced by cosmic rays passing through the detector. The signals are not from the same ionization event as can be inferred by noting the difference in the arrival time. TODO: Clean up the figure

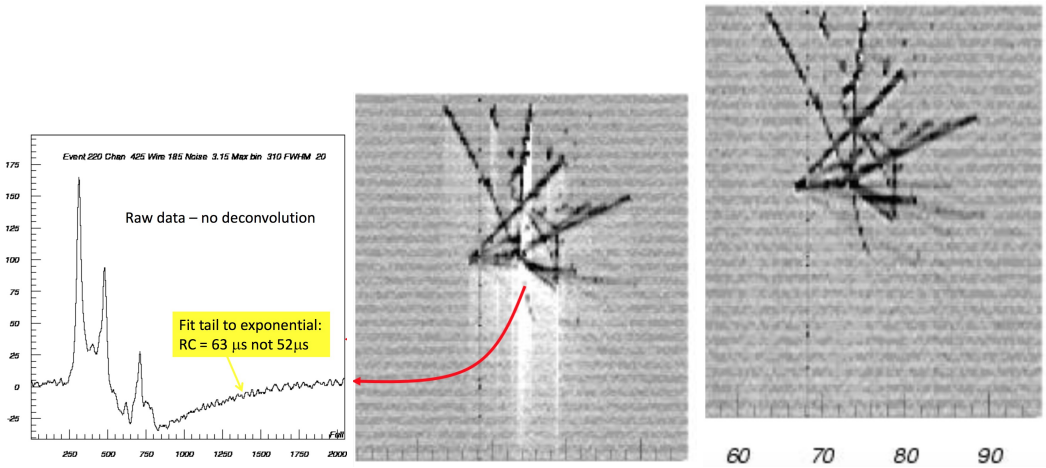

Figure 5. Neutrino interaction with secondary hadronic interaction in the ArgoNeuT detector. Data taken in the NuMI beam in 2009. Left: Raw ADC value vs time tick (1 tick = 0.2 μs) for a wire in a high ionization region in the collection plane. The RC time constant of the tail was found to be 63 μs instead of 52 μs from bench measurement. Middle: Time vs wire number (wire spacing = 4 mm). The image grey scale is based on the raw ADC values before deconvolution. The white regions show a baseline shift due to poor matching to the readout electronics. Right: The same event after deconvolution. TODO: figures need cleanup

3. Offline Signal Processing

Several detector features and electronics artifacts were described in the previous section that can

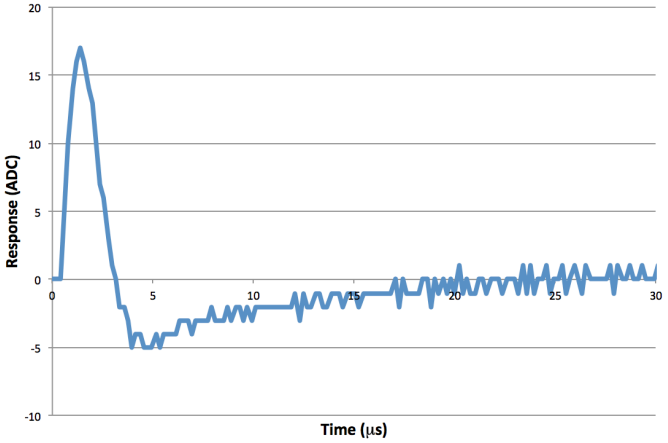

Figure 6. Left: Response of the ArgoNeuT preamplifier to a δ-function input. The scatter in the points is due to digitization error of the ADC. Right:

be removed by offline signal processing. The digitized signal is a convolution of the serial effects of signal formation, electron transport through the main volume and wire planes and processing by the readout chain as shown schematically here: Signal = Ionization $\otimes$ Recombination $\otimes$ Diffusion and Attachment $\otimes$ Field $\otimes$ Noise $\otimes$ Electronics. In this section we describe a wire signal Fourier deconvolution method that remove some of these artifacts to prepare signals for hit finding.

This method also provides the opportunity to eliminate coherent noise using a Wiener filter. It is important that the filter does not unintentionally remove components of the wire signal however. Using a Gaussian approximation, the width of a wire signal in the frequency domain, $\sigma_f = 1/(2\pi\sigma_t)$, where σ_t is the width in the time domain. The signal is maximum at $f = 0$. An estimate of the high frequency cut-off can be made by observing that the highest frequency component of the wire signal is related to the inverse of the transit time through the wire plane gap. Using an example where σ_t = 2 μs, a low-pass Wiener filter should have a $3\sigma_f$ cut-off at $\approx$200 kHz.

Electronics Response: The electronics response due to a δ-function is generally obtained from simulations and bench tests. Figure 6 shows the output of the ArgoNeuT preamplifier when a δ-function signal is injected. (TODO: reference?) The data were taken with a 10 bit ADC sampled at 198 ns/tick. The noise rms was $\approx$1 ADC count as can be inferred by the jitter on the long tail. The large baseline shift shown in Figure 5 is due to the negative lobe of the preamplifier response near 5 μs.

Field Response: Determining the field response appears to be more complicated. Ionization electrons follow complex 3D trajectories as they pass through the wire planes producing direct and induced signals on nearby wires. Signals are also induced on next-to-neighbor wires due to inter-wire capacitance but this is in general not observed since they are of similar magnitude to the series noise from the wire capacitance. An additional complication is that the detailed shape of the field response depends on the wire bias voltage settings. In practice it is sufficient to model the field response with a simple analytic form that can be scaled for different operating conditions. A suitable analytic form can be developed by doing a comparative study of simulated and real wire signals. TODO: USE ARGONEUT STUDY AS AN EXAMPLE IN AN APPENDIX?

Diffusion and Attachment: The effects of diffusion are small and not calculable unless the event time, t_o, is known a priori. Using MicroBooNE as an example, the longitudinal and transverse diffusion rms for electrons traveling the full 2.5 m drift is 1.3 mm and 2 mm respectively corresponding to an increase in the time spread of 1 tick. Likewise, correcting for electron attachment requires knowledge of t_o and is a simple multiplicative factor that can be applied in later stages of reconstruction.

Recombination: A recombination correction is required for calorimetric reconstruction but requires knowledge of the path length of the track in space to calculate dQ_o/dx. Applying a recombination correction to electromagnetic showers requires a somewhat different approach. A reasonable approximation is to assume that all charge in the shower is attributed to electrons, all of which are minimum ionizing particles. A constant value of $\mathscr{R} \approx 0.63$ for a MIP is reasonable.

The approach described here is to remove the electronics response and field response, resulting in wire signals that are roughly Gaussian in shape for a track that is parallel to the wire plane. In this situation, all of the ionization electrons arrive at the wire plane at roughly the same time. Therefore a fit to a Gaussian distribution provides a good estimate of the hit position and the ionization charge. Ionization electrons produced on tracks that travel roughly in the electric field direction, $\phi \rightarrow 0$, will arrive over many microseconds. In this case a single Gaussian fit will not be sufficient. An extreme example from the ArgoNeuT data is shown in Figure 7 in which $\phi = 0$. A Gaussian fit would clearly not provide the information required to reconstruct this track.

Signal deconvolution has become a standard feature of the wire calibration module in LArSoft along with a predecessor algorithm that identifies a "Region of Interest", ROI, for a prospective hit. A ROI is a block of consecutive ADC samples which are above (below) a positive (negative) noise threshold plus pre-padding and post-padding with some number of ADC samples. Deconvolution is applied to each ROI with a kernel prepared for that wire plane and ROI length. Figure 8 shows an example of a simulated MicroBooNE V-plane raw signal and the result after application of the ROI finding algorithm, deconvolution and local baseline subtraction. The ROI algorithm significantly reduces the amount of data that needs to be stored for later processing and results in a Gaussian-like shape that is amenable to hit fitting.

4. Hit Reconstruction

Hit reconstruction is a seemingly straightforward process of characterizing the position and amount of charge deposited in the detector within each ROI. The charge is the simply the integral of a wire signal ROI. The hit time relative to t_o can be calculated using the charge weighted mean of the ROI. Information that could be used to separate close tracks or complicated ionization events would be lost using this simple procedure however. The method described here improves the reconstruction of track hits - in particular those close to a neutrino interaction.

Each ROI is fit to a variable number of Gaussian distributions each defined by a time, peak amplitude and width, σ. The first step in the algorithm is to find a set of local maxima in the ROI above a threshold. An initial fit of the Gaussian distributions is performed assuming $\sigma_{noise} = 1$ ADC count. A χ^2/DOF scaling factor is provided to compensate for a non-Gaussian field response and for $\sigma_{noise} \neq 1$. The scaled χ^2/DOF of the fit is used to decide whether to continue fitting with additional "hidden" Gaussian distributions or to create a "crude hit" that encapsulates the global

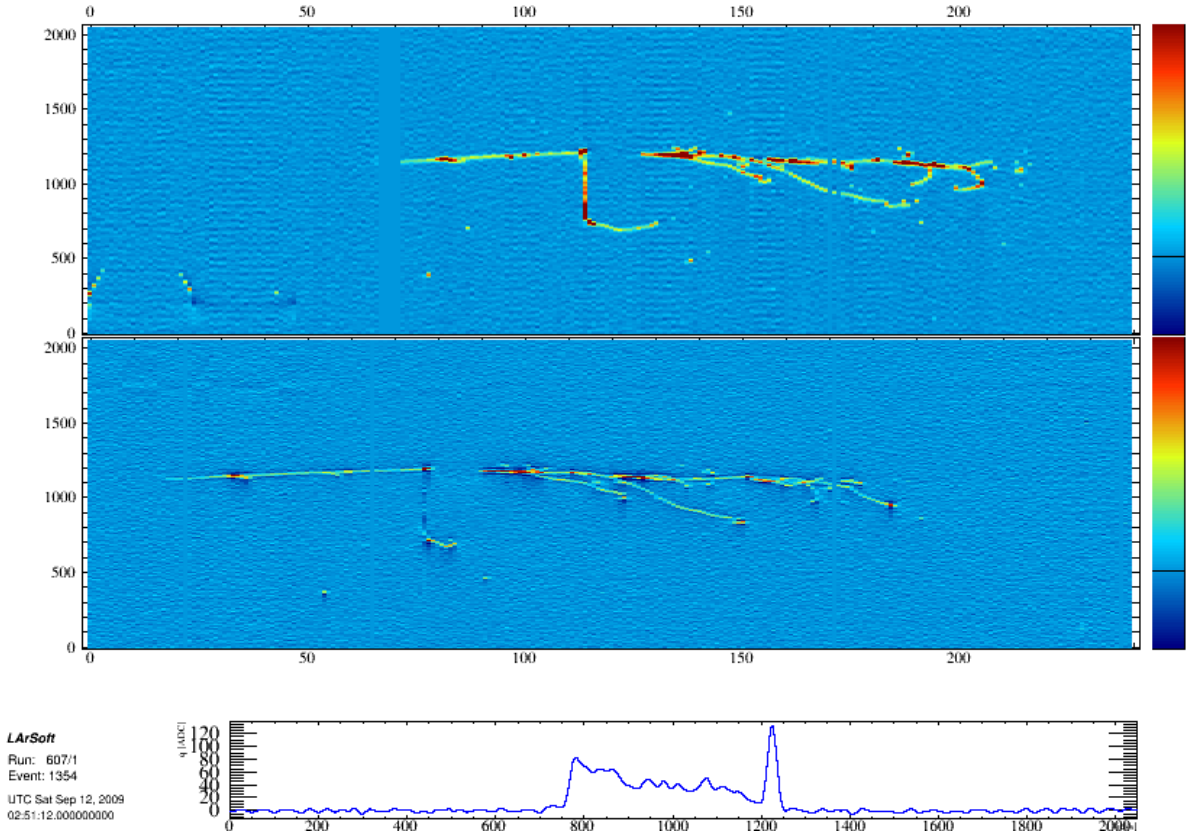

Figure 7. Top: Collection plane view of a particle entering the ArgoNeuT detector producing a particle that travels along the electric field direction towards the anode plane (vertical in this view). The particle travels for 10 cm before it decays or re-interacts. Bottom: ADC vs time of the collection plane wire along which the particle travels. The large peak near 1200 ticks is due to low energy particles produced in the collision. Ionization fluctuations along the particle trajectory are apparent as it travels from 1200 $\rightsquigarrow$ 800 ticks. Middle: Induction plane view showing the (expected) negligible signal. The wire signals are shown after deconvolution.

features of an ionization event in this ROI and passes it to downstream modules. The signal in Figure 7 clearly falls in the latter category.

The properties of a hit are simply the parameters from the Gaussian fit. The number of ionization electrons, or "hit charge" Q_{hit}, is proportional to the area. A hit is a member of a "multiplet" if it was found in a multi-Gaussian fit. Figure 9 illustrates the rationale for introducing this concept. The top panel shows the trajectory of a simulated low momentum particle in a collection plane view in MicroBooNE. Gaussian fits to the charge deposited on two adjacent wires are shown in the middle and lower panels. A good fit to five Gaussian distributions was found on one wire which resulted in a multiplet of five hits. A good fit to one Gaussian distribution was found on the adjacent wire resulting in one hit. The hits on these two wire were reconstructed from the same ionization event but are

It is evident that there is insufficient information at this stage of reconstruction to make an

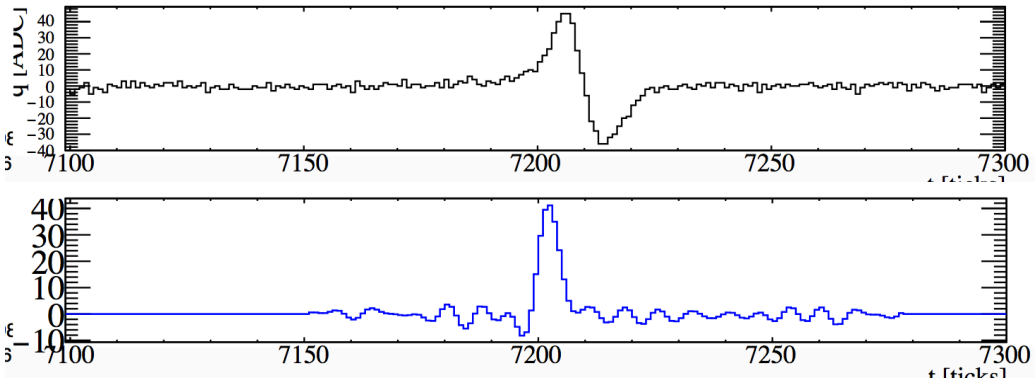

Figure 8. Top: Simulated raw signal in the V plane of a shallow angle track in MicroBooNE. Bottom: After deconvolution. The ROI consists of the region 7155 ⇝ 7280 ticks.

unambiguous definition of a hit that can be used with confidence by later stages of reconstruction. The 5-hit multiplet in this Figure could conceivably have been created by multiple tracks created in a neutrino interaction or a secondary interaction. The cluster algorithm described in the next section resolves this type of ambiguity by merging hits in a multiplet if they are embedded in a large angle cluster but preserves the multiplet if it is not.

A second type of ambiguity arises when charge from multiple tracks overlap and are fit as a single Gaussian hit. This occurs at the primary vertex of every neutrino interaction to some degree. One negative consequence is that pattern recognition of tracks near a vertex will be incorrect. A second negative consequence is that dQ/dx of any reconstructed short tracks will be erroneously large. Untangling the effects of overlapping tracks should potentially allow the identification of MeV-scale particles produced by final state interactions. Techniques for resolving this ambiguity are in their infancy and are described in section 8.

5. Cluster Finding

The term "cluster" in this document refers to a line-like collection of hits in a wire plane such as that shown in the top panel of Figure 9. The algorithm is loosely based on the concept of a cellular automata glider. Tracking decisions are made using the position (W, T) of a hit on the cluster, the local slope (S = dT/dW) and the local average hit charge, Q_{ave}. Here T is the time in ticks and W is the wire number. Cluster parameters are updated as hits are added to the cluster.

Tracking begins by finding a seed cluster at the downstream end of a plane in the TPC where the density of particles produced in a neutrino interaction is expected to be the lowest. The cluster begin slope, slope error and charge are calculated at the most downstream hit. The expected time of a hit on the next upstream wire is calculated. A time window for accepting a hit is calculated using cluster parameter errors and a user defined factor. A hit on this wire is appended to the leading edge of the seed cluster if a linear fit to all hits in the cluster results in an acceptable χ^2.

Some complexity is added to this trivial scheme after the cluster reaches a length where a linear fit to all cluster hits, N_{Hits}, is no longer suitable and where trends in the hit charge can be estimated. Two user-defined parameters, $N_{HitsFit}$ and $N_{HitsAve}$ trigger the start of these calculations. A linear fit is performed with $N_{HitsFit}$ hits on the leading edge of the cluster to find T_{fit} and S_{fit} at

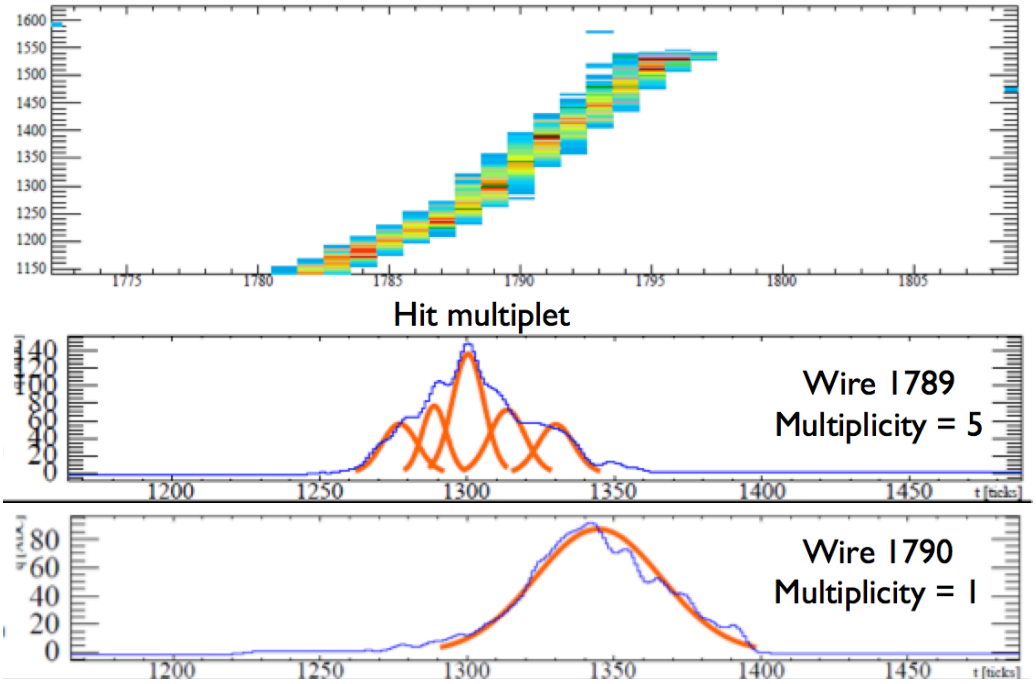

Figure 9. Top: A large angle cluster of hits. Middle: A multiplet of 5 hits created on wire 1789. Bottom: A single hit created on the next wire.

the most upstream hit. Another fit is performed with $N_{HitsAve}$ hits on the leading edge of the cluster to find Q_{ave} and dQ_{ave}/dW. The values of $N_{HitsFit}$ and $N_{HitsFit}$ can be varied as described below to track long straight muons as well as short stopping electrons and pions.

The cluster position is extrapolated to the next upstream wire and a search for the next cluster hit is made. Tracking stops if there is no hit in the search window.

6. Vertex Finding

7. Track Finding

8. Future Prospects

A. Appendix A - LArTPC Calculator

TODO: This should be in an appendix.

The LArTPC calculator is an Excel spreadsheet that can be used to estimate LArTPC performance. The user enters detector parameters such as the wire spacing, wire diameter, drift electric field, etc, in the un-shaded cells. The wire signal amplitude on the collection plane produced by an idealized "track" that travels perpendicular to the wire plane is calculated. The calculator utilizes a parameterization of the BNL preamplifier ASIC[**?**], an intermediate amplifier and sampling ADC to estimate the signal to noise ratio.

Derived quantities such as the drift electron velocity, maximum drift time, signal to noise ratio, etc are displayed in blue shaded cells. Non-scaling parameters of liquid argon such as the ionization energy, diffusion coefficient, etc are highlighted by the salmon colored cells.

The calculator accounts for the electric field dependence of the electron drift velocity. The charge loss due to recombination is calculated using both Birk's Law and Modified Box Model formulae.

The calculator is available at no cost. Please contact the author within the next 24 hours to receive your own FREE calculator. TODO: Seriously, what is the protocol for doing this?

Acknowledgments

Acknowledgments.

References

[1] G. Jaffe, *The columnar theory of ionization*, *Ann. Phys.* **42** (1913) 303.

[2] S. Amerio et al., *Design, construction and tests of the ICARUS T600 detector*, *NIM* **A527** (2004) 329.

[3] C. Anderson et al., *The ArgoNeuT Detector in the NuMI Low-Energy beam line at Fermilab.*, 2012 *JINST* **7** P10019.

[4] The MicroBooNE collaboration, *The MicroBooNE Technical Design Report?*, *xxx* **yyy** (1901) 666.

[5] S. Claus et al., *LArSoft* , *xxx* **yyy** (1901) 666.

[6] M. Wojcik and M. Tachiya, *Electron thermalization and electron-ion recombination in liquid argon*, *Chem. Phys. Lett.* **379** (2003) 20.

[7] G. Jaffe, *The columnar theory of ionization*, *Ann. Phys.* **42** (1913) 303.

[8] J. B. Birks, *Proc. Phys. Soc.* **A64** (1951) 874.

[9] S. Amoruso et al., *Study of electron recombination in liquid argon with the ICARUS TPC*, *NIM A* **523** (2004) 275.

[10] J. Thomas and D.A Imel, *Recombination of electron-ion pairs in liquid argon and liquid xenon*, *Phys. Rev. A* **36** (1987) 614.

[11] B. Baller, *A study of electron recombination using highly ionizing particles in the ArgoNeuT Liquid Argon TPC.*, 2013 *JINST* **8** P08005.

[12] A. M. Kalinin, et al., *Temperature and electric field strength dependence of electron drift velocity in liquid argon ATLAS Internal Note* **LARG-NO-058** (1996).

[13] O. Buneman et al., *Design of grid ionization chambers*, *Can. J. Res.* **A27** (1949) 191.

[14] G. Horton-Smith, *Wire Plane Analytic Calculations - To be Published?*, *uB doc 4708* (2015).

Enter detector values in blank cells
Blue cells contain derived quantities
Salmon cells contain non-scaling properties
Version 3, October 9, 2015
Bruce Baller (baller@fnal.gov)

"LarProp" = Craig Thorn's "LAr Properties V9a", uB doc #412, LBNE doc #4482

Detector Properties	Value	Units	Notes
Max drift distance	2.56	m	
Drift E field	0.5	kV/cm	
Electron drift velocity	1.6	mm/micro-sec	Walkowiak, ref uB doc #342
Max electron drift time	1.6	ms	
Ion drift velocity	0.8	cm/s	
Max ion drift time	320	s	
Gap 1 E-Field for full transparency	0.75	kV/cm	
Gap 1 drift velocity	1.8	mm/micro-sec	
Gap 2 E-Field for full transparency	1.13	kV/cm	
Gap 2 drift velocity	2.1	mm/micro-sec	
Wire spacing	3	mm	
Wire diameter	0.15	mm	
Min E-Field ratio for 100% transparency	1.37		Buneman, Canadian J. Res. Vol 27, p 192-208. Analytical form for 2D wire planes
E Field ratio setting	1.50		Should be set somewhat higher than the derived quantity above
Wire plane gap	3	mm	
Wire capacitance in air	16	pF/m	includes 5 pF of parasitic capacitance for wire attachment
Wire length	10	m	
Wire capacitance in LAr	243	pF	
Cathode High voltage	-128	kV	
Bias voltage - Induction 1	-225	V	
Bias voltage - Induction 2	0	V	Assumed virtual ground
Bias voltage - Collection	338	V	
Front end amplifier shaping time	2	micro-sec	BNL ASIC choices (0.5, 1, 2, 3)
ADC sampling rate	2	MHz	
Sample time	0.50	micro-sec	
Front end amplifier gain	7.8	mV/fC	BNL ASIC choices (4.7, 7.8, 14, 25)
ADC scale factor	2.0	ADC counts/mV	Nevis uB electronics
Electron lifetime - assumption	6	ms	
Equivalent O2 contamination	53	ppt	
Number of MIPs - assumption	1		

General (LAr) Properties			
LAr Temperature	89	K	
LAr Density	1.38	g/cm^3	LArProp
Dielectric constant	1.51		
W ion - ionization energy	23.6	eV/ion	
W photon	19.5	ev/photon	
dE/dx for Number of MIPs - assumption	2.07	MeV/cm	Bethe-Bloch: One MIP deposits 1.498 MeV cm^2/g
Recombination - Birks	0.70		Amoruso, et al NIM A 523 (2004) 275
Recombination - Modified box model	0.71		Baller, 2013 JINST 8 P08005
Photon recombination factor	0.44		LArProp
Ion mobility	0.0016	cm^2/V-s	LArProp
Diffusion coefficient - Long	5	cm^2/s	LArProp
Diffusion coefficient - Trans	13	cm^2/s	

Electronics Signal & Noise			
Ionization after recombination	18348	electrons	Ionization produced one wire by track traveling perpendicular to it
Front end amplifier Signal - Collection	23	mV	
Signal ADC counts - Collection	47	counts	
ENC 90K	472	electrons	BNL ASIC
ENC 90K	1.2	counts rms	
ENC 300K	532	electrons	BNL ASIC at room temperature
Signal to noise ratio - max	39		
Signal to noise ratio - min	30		
Induction 2 signal width estimate	1.6	micro-sec	Rough estimate w/o electronics shaping or electron arrival time spread
Collection signal width estimate	0.7	micro-sec	Rough estimate w/o electronics shaping or electron arrival time spread

Diffusion			
Longitudinal diffusion rms - max	1.3	mm	
Longitudinal diffusion rms - max	1.0	ADC samples	
Transverse diffusion rms - max	2.0	mm	

Scintillation Light			
Photon yield	46558	photons/cm	

Figure 10. blah blah.